Mathematical Geology, Vol. 33, No. 3, 2001

Extended Self-Similarity in Geophysical and Geological Applications[1]

Vladimir I. Nikora[2] and Derek G. Goring[3]

In this paper we demonstrate application of the Extended Self-Similarity (ESS) concept, recently developed in turbulence physics, for geological and geophysical phenomena. The theoretical background is discussed first and then the ESS properties in fluvial turbulence, sand wave dynamics, Martian topography, river morphometry, gravel-bed mobility, and atmospheric barometric pressure are explored. The main attention is paid to fluvial turbulence and sand waves, while other examples are presented to support the generality of the ESS concept in earth sciences. The results show that the ESS properties of the considered phenomena are remarkably similar to those reported for turbulence, in spite of different underlying mechanisms. This suggests that a general rule should exist which governs a wide class of complex natural phenomena.

KEY WORDS: self-similarity, scaling, intermittency, turbulence, sand waves, Martian surface.

INTRODUCTION

Very often geological and geophysical objects and processes show similarity at various spatial and temporal scales. Although this important property has been recognized for many decades, only recently has it received massive attention, and as a result, the geological literature has been flooded with new ideas and discoveries dramatically challenging existing knowledge of Earth systems (e.g., Turcotte, 1997). Such a success would not be possible without scaling ideas and concepts developed in physics and quickly penetrated into geological sciences. Many of these ideas relate to the self-similarity concept, which means reproducing itself on different time and spatial scales (Barenblatt, 1979). This concept is a basis or a necessary part of fractal methodology, self-organized criticality, renormalization methods, percolation models, and chaotic systems that have become familiar

[1]Received 28 July 1999; accepted 1 February 2000.
[2]National Institute of Water and Atmospheric Research (NIWA), P. O. Box 8602, Christchurch, New Zealand, 8034. e-mail: v.nikora@niwa.cri.nz
[3]National Institute of Water and Atmospheric Research (NIWA), P. O. Box 8602, Christchurch, New Zealand, 8034. e-mail: d.goring@niwa.cri.nz

0882-8121/01/0400-0251$19.50/1

tools in earth sciences. Indeed, today it is widely recognised that self-similarity, or scale-invariance, of geological phenomena is the rule rather than an exception.

Although, in general, self-similarity may be expressed in several different ways it is often manifested mathematically as a power function $y(x) = ax^{\beta}$, which obeys the homogeneity relation $y(\lambda x) = \lambda^{\beta} y(x)$, where λ is a (positive) scale factor, and β is a scaling exponent. Functions that satisfy this relation are said to be *scaling functions* while processes or objects that are described by such functions are said to exhibit *scaling behavior*. With this, the terms *scaling*, *scale-invariance*, and *self-similarity* are often used as interchangeable terms. There are numerous examples of power relationships between geological variables (Turcotte, 1997), though the ranges of reported scaling behavior are often less than one order of magnitude. Actually, this is not surprising, as scaling behavior in nature is always limited between internal (small) and external (large) scales introduced by the driving mechanisms or by structural properties. A good example may be found in turbulence where classical Kolmogorov's scaling (Monin and Yaglom, 1975; Frisch, 1995) is constrained by viscosity at small scales and by the flow size at large scales. With limited data, such constraints introduce unavoidable uncertainties in the identification of true scaling behavior or scaling regions (Avnir and others, 1998).

This problem, until recently, has been a stumbling block for turbulence researchers studying scaling properties of developed (high Reynolds number) turbulence. In 1993 Benzi and others (1993a,b) introduced the concept of extended self-similarity (ESS), as a generalized form of scale-invariance. Using a special kind of data presentation they discovered that the range of scaling behavior was significantly extended in comparison with conventional scaling analysis. In the following years this concept has been extensively used in scaling studies of turbulence and, moreover, it has been suggested that ESS scaling exponents are possibly more "fundamental" than conventional ones (Biferale, Benzi, and Pasqui, 1997). Very recently, ESS has been successfully applied to study scaling properties in diffusion-limited aggregates (Queiros-Conde, 1997), natural images (Turiel, Mato, and Parga, 1998), and kinetic surface roughening (Kundagrami and others, 1998). Although these problems are different from three-dimensional (3D) fluid turbulence in nature, they all show the existence of ESS properties remarkably similar to those in turbulence.

In this paper we extend the application of the ESS concept to geological and geophysical phenomena by exploring potential ESS properties in (1) fluvial turbulence, (2) sand wave dynamics, (3) Martian topography, (4) river morphometry, (5) gravel-bed mobility, and (6) atmospheric barometric pressure. The selection of these phenomena has been driven by our research interests and availability of data. In our analysis, we focus on fluvial turbulence and sand waves. Other examples are discussed only briefly and are presented to support the generality of the ESS concept to earth sciences. We devote this paper to the memory of the Late Professor

S. V. L. N. Rao, who promoted different directions in mathematical geology and whose life may serve as an example of outstanding service to science.

BACKGROUND

In 1941 Kolmogorov introduced the structure function as a tool to study small-scale turbulence (Monin and Yaglom, 1975; Frisch, 1995):

$$D_{Kp}(r) = \langle \Delta u(r)^p \rangle \tag{1}$$

where $\Delta u(r) = [u(x_i + r) - u(x_i)]$ is the velocity increment between two points lying on the x_i-axis and separated by distance r, p is the order of the structure function, and angular brackets define averaging over many points. Many geologists are familiar with the second-order structure function with $p = 2$ in (1) which is a popular tool in geology well-known as the semivariogram or variogram (Davis, 1986). For r from the inertial subrange of scales (i.e., much less than the external flow scale and much larger than the scale where dissipation occurs) Kolmogorov's initial theory (referred to hereafter as K41) predicts the following relationship for the longitudinal structure function:

$$D_{Kp}(r) = c_p \bar{\varepsilon}^{p/3} r^{\xi(p)} \tag{2}$$

where the constants c_p are presumed to be "universal," $\bar{\varepsilon}$ is the mean energy dissipation, and $\xi(p) = p/3$. Relationship (2) exhibits *simple* or *ordinary scaling* in eddy structure within the inertial subrange. The deviation of measured exponents $\xi(p)$ from $p/3$ (especially profound for large p) has inspired revisions of K41, which incorporate intermittency in the velocity, vorticity, and/or dissipation fields (Frisch, 1995). To account for intermittency, the revised expression for the velocity structure function in the inertial subrange can be presented as

$$D_{Kp}(r) = c_p^* \bar{\varepsilon}^{p/3} L_o^{p/3-\xi(p)} r^{\xi(p)} \tag{3}$$

where the definition of exponents $\xi(p) \neq p/3$ depends on the particular intermittency model, L_o is the external turbulence scale (e.g., integral scale), and the c_p^* is a new set of constants related to c_p as $c_p = c_p^*(L_o/r)^{p/3-\xi(p)}$. Relationship (3) exhibits *multiscaling* due to intermittency, which means that $\langle \Delta u(r)^p \rangle$ does not scale in the same way as $\langle \Delta u(r)^2 \rangle^{p/2}$, in contrast to the simple scaling in (2). Note that the term *multiscaling* also refers to the effect upon p of dependence of crossover between the inertial subrange scaling and dissipative range scaling. Until recently, Kolmogorov's structure functions have been used directly as tools for testing various intermittency models. However, Benzi and others (1993a,b)

found that much better estimates for the inertial-range scaling exponents $\xi(p)$ can be achieved by using the self-scaling properties of structure functions, i.e.,

$$D_{Kp}(r) = m_p |D_{K3}(r)|^{\xi^*(p)} \tag{4}$$

where m_p are constants independent of r, $D_{K3}(r) = \langle \Delta u(r)^3 \rangle$, and the "relative" exponents $\xi^*(p)$ are assumed to be equal to $\xi(p)$. The reason for this assumption is the linearity of the relationship $D_{K3}(r) = -(4/5)\bar{\varepsilon} r$, which Kolmogorov derived rigorously from the Navier–Stokes equations. Benzi and others (1993a,b) have also suggested that relationship (4) be valid for moments of the absolute values of velocity increments, i.e.,

$$D_{Gp}(r) = m_p^* D_{G3}^{\xi'(p)}(r) = m_p^{**} |D_{K3}(r)|^{\xi^{**}(p)} \tag{5}$$

where $D_{Gp}(r) = \langle |\Delta u(r)|^p \rangle$ are the so-called generalized structure functions, m_p^* and m_p^{**} are new sets of constants, and $\xi^*(p) = \xi'(p) = \xi^{**}(p)$ are assumed. The latter equalities are only valid if $|D_{Kp}(r)| \propto D_{Gp}(r)$, which is automatically true for even integer orders. In a recent paper we have shown that $|D_{Kp}(r)| \propto D_{Gp}(r)$ is also valid for odd p if r is from the inertial subrange (Nikora and Goring, 1999a). In relationships (4) and (5) the p-order structure functions relate to the third-order structure function. However, in general, the ESS scaling has a form $D_{Gp}(r) = m_{np} D_{Gn}^{\xi'(n,p)}(r)$ where exponents $\xi'(n, p)$ are called the relative ESS exponents.

Benzi and others (1993a,b) discovered that ESS, as presented by (4) and (5), survives in the range from the integral scale L down to mildly dissipative scales of the order of 5η where η is Kolmogorov's scale of dissipative eddies. This contrasts with the ordinary scaling represented by (2) and (3), which is known to fade away at much larger scales, of the order of $(25–35)\eta$ or more. To explain this effect, Benzi and others (1993b) proposed the following scaling relationship:

$$D_{Gp}(r) = A_p U^p [(r/L) f(r/\eta)]^{\xi(p)} \tag{6}$$

where U is some characteristic velocity of the flow. The function $f(r/\eta)$ is responsible for viscosity effects and explains why ESS is extended toward small scales (beyond the classical cutoff of the inertial subrange at $\approx 25–35\eta$). This property of ESS explains the origin of the name Extended Self-Similarity. It has been also found that ESS holds at high Reynolds numbers as well as at moderately low Reynolds numbers. Such behavior is also different from ordinary scaling, which assumes fully developed turbulence (i.e., Re tends to infinity). Since the introduction of ESS many researchers have tested this approach and found that ESS improves scaling estimates enormously, though recognizing that it is not fully understood why this is so (see Benzi and others, 1996, or Biferale, Benzi, and Pasqui,

1997, for review). As a further development of ESS, Benzi and others (1996) have introduced its generalized form, the so-called generalized extended self-similarity (G-ESS), i.e.,

$$G_p(r) = G_q(r)^{\rho(p,q)} \tag{7}$$

where $G_p(r) = D_{Gp}(r)/D_{G3}(r)^{p/3}$, $G_q(r) = D_{Gq}(r)/D_{G3}(r)^{q/3}$, and $\rho(p, q) = [\xi(p) - \xi(3)p/3]/[\xi(q) - \xi(3)q/3]$ by definition. They also provided an explanation for G-ESS based on generalization of turbulence phenomenology. It has been found that relationship (7) describes various turbulence data even better than do (4) and (5). In general, the G-ESS scaling can be presented as

$$G_{np}(r) = G_{nq}(r)^{\rho(n,p,q)} \tag{8}$$

where $G_{np}(r) = D_{Gp}(r)/D_{Gn}(r)^{p/n}$, $G_{nq}(r) = D_{Gq}(r)/D_{Gn}(r)^{q/n}$.

Originally, the ESS and G-ESS concepts have been developed to describe single-valued functions, like velocities $u(\mathbf{x}, t)$, by means of the generalized structure functions (5) and (7). However, applicability of these concepts is not limited to structure functions only, and may be equally successful when applied to statistical moments of a different nature. For example, Queiros-Conde (1997) used the ESS concept to explore scaling properties of diffusion-limited aggregates (DLA) by means of statistical moments $\sigma_p = \langle |R - \langle R \rangle|^p \rangle$, analogous to (1), where R is the distance between a particle in a DLA cluster and the seed (or origin) of the cluster. It would be interesting to apply such an approach for river networks, which are similar, at least topologically, to DLA. However, in this paper we restrict ourselves to geological phenomena that can be described with single-valued functions and with ESS/G-ESS applied to their structure functions. Before presenting these data, we briefly describe a procedure that is helpful in distinguishing between intermittent (or *multiscaling*) and nonintermittent (or *simple scaling*) behavior.

PHASE RANDOMIZATION TEST OF INTERMITTENT BEHAVIOR

One application of the ESS concept is to the evaluation of the scaling exponents $\xi'(p)$ and the identification of potential multiscaling behavior due to intermittency, i.e., the nonlinearity of $\xi'_p = f(p)$. The latter can be assessed by defining confidence intervals for $\xi'(p)$, which is not a trivial task. Alternatively, one can define a probability P that the measured exponent $\xi'_m(p)$ is not distinguishable from the "nonintermittent" exponent $\bar{\xi}'_n(p)$, where the overbar denotes an average value from N estimates of $\xi'_n(p)$. In other words, one can formulate the null hypothesis

as H_o: $\xi'_m(p) = \bar{\xi}'_n(p)$, and use the normally distributed random variable:

$$V = \frac{[\bar{\xi}'_n(p) - \xi'_m(p)]}{\sigma(\xi'_n)} = \frac{[\bar{\xi}'_n(p) - \xi'_m(p)]\sqrt{N}}{\sigma_{\xi_n}} \tag{9}$$

as a criterion to test this hypothesis. Equation (9) assumes that $\xi'_n(p)$ is a normally distributed random variable. If the null hypothesis is correct we have $E[V] = 0$ and $\sigma(V) = 1$. To apply this approach, we first need to calculate V_c using (9), and second, to compare V_c with V_{cr} for a given significance level p_o. The value of V_{cr} should be defined from (e.g., Bendat and Piersol, 1986):

$$F(V_{cr}) = (1 - p_o)/2, \quad \text{where } F(x) = \frac{1}{\sqrt{2\pi}} \int_0^x e^{-z^2/2}\, dz \tag{10}$$

If $|V_c| < V_{cr}$, the null hypothesis, H_o: $\xi'_m(p) = \bar{\xi}'_n(p)$, should be accepted at the significance level p_o (i.e., the scaling is simple); if $|V_c| > V_{cr}$, the null hypothesis should be rejected, which means $\xi'_m(p) \neq \bar{\xi}'_n(p)$, i.e., multiscaling exists. To apply this approach one would need estimates for the nonintermittent exponents $\xi'_{ni}(p)$. These can be obtained using the phase-randomization procedure (Yamada and Ohkitani, 1991; Goring and Nikora, 1999). Phase-randomized counterparts of measured geophysical signals are derived by inverse transform of the Fourier coefficients of the initial data, after randomizing their phases uniformly between 0 and 2π but keeping their amplitudes unchanged. The phase-randomization procedure destroys intermittency, if any, in the initial data and produces new, nonintermittent Gaussian data sets with the same spectra and the second order structure functions as for the initial signals, i.e., $\bar{\xi}'_n(2) \equiv \xi'_m(2)$. Thus, one can obtain as many estimates of $\xi'_{ni}(p)$ as necessary. Our Monte Carlo simulations confirm that, indeed, $\xi'_{ni}(p)$ is a normal distributed random variable. The mean exponent $\bar{\xi}'_n(p)$ is connected with $\xi'_m(2)$ as $\bar{\xi}'_n(p) = [\xi'_m(2)/2]p$. We use the described method in this study as a routine to distinguish ordinary scaling from multiscaling.

FLUVIAL TURBULENCE

To explore the ESS/G-ESS properties of fluvial turbulence, we use the longest (20 min) measurements from our data set measured in the Balmoral Irrigation Canal with a weakly mobile gravel bed (North Canterbury, New Zealand). The cross-sectional shape of the channel is close to trapezoidal with top width of 6.2–7.0 m and bottom width of 3.5–4.5 m. To minimise side-wall effects, all measurements were in the central part of the flow. The main hydraulic parameters for the experiments were: flow rate $Q = 5.14$ m^3/s; hydraulic radius $R = 0.70$ m; global Reynolds number $\mathrm{Re} = U_a R/\nu = 0.74 \times 10^6$ where U_a is cross-sectional

mean velocity; global Froude number $Fr = U_a/\sqrt{gR} = 0.40$; and friction velocity $u_* = 6.94$ cm/s (obtained from Reynolds stress measurements). The depth at the measuring vertical was $H = 1.05$ m. The measurements were conducted using 3D Acoustic Doppler Velocimeters (ADV) with the sampling volume 10 cm beneath the transducer (Kraus, Lohrmann, and Cabrera, 1994; Nikora and Goring, 1998), with a sampling interval of 0.04 s. The experimental procedure, field site characteristics, and data analysis are detailed in Nikora and Goring (1999b). To recover spatial structure functions from temporal structure functions, we use Taylor's frozen turbulence hypothesis, which was specially tested for this data set (Nikora and Goring, 2000a). In our analysis we consider the longitudinal structure functions for longitudinal (downstream) velocities measured at two points, with distance from the bed $z = 0.8$ cm (high-shear turbulence) and $z = 49$ cm (low-shear turbulence).

Analysis of the third order Kolmogorov's structure function $D_{k3}(r)$ shows that the region where $D_{K3}(r)/r \approx const$ (which indicates the inertial subrange scaling) does not exist in the high-shear near-bed region ($z = 0.8$ cm), but is quite observable in the low-shear region, at $z = 49$ cm (Fig. 1A). However, the ESS plots demonstrate well-observable scaling with the same exponents for both measuring points, at least at small spatial lags (actually the difference between two groups of exponents, for $z = 0.8$ and 49 cm, is less than 2.7%). These exponents appeared to be very close (within 0.2–2.2%) to those derived in She and Leveque's (1994) hierachical structure model. Note that their exponents provide, to date, the best fit for homogeneous turbulence data. An important property of the plots in Figure 1C for $z = 49$ cm is that the ESS scaling regions cover not only the inertial subrange, but significantly extend toward larger scales, well above the upper boundary of the inertial subrange indentified in Figure 1A. Moreover, the ESS also shows well-defined scaling at $z = 0.8$ cm with the same ESS exponents as for $z = 49$ cm, though no scaling has been identified for the ordinary presentation of structure functions, Figure 1A. For both $z = 0.8$ and 49 cm, the large-scale boundaries for the ESS scaling are significantly beyond the integral scales, which can be approximately represented for our case study by the distance from the bed. The phase-randomized structure functions follow $D_{Gp}(r) \propto r^{[\xi(2)/2]p}$, as one would expect, that gives ESS scaling $D_{Gp}(r) \propto [D_{G3}(r)]^{p/3}$ equivalent to pure K41 scaling without intermittency (Figs. 1D and 1E). Indeed, deviations of fitted exponents from $p/3$ are less than 0.5%. Note that ESS covers not just the inertial subrange, but the whole range of scales investigated (Figs. 1D and 1E).

The above results suggest that a more general form of relationship (6) should be used to account for large-scale (i.e., $r > L$) extension of ESS, i.e.,

$$D_{Gp}(r) = A_p U^p [\, f(r/\eta, r/L)]^{\xi(p)} \tag{11}$$

where $f(r/\eta, r/L) = r/L$ for $\eta \ll r \ll L$. For $r > L \gg \eta$ the function $f(r/\eta, r/L) = f_1(r/L)$ accounts for large-scale nonuniversal flow properties that are

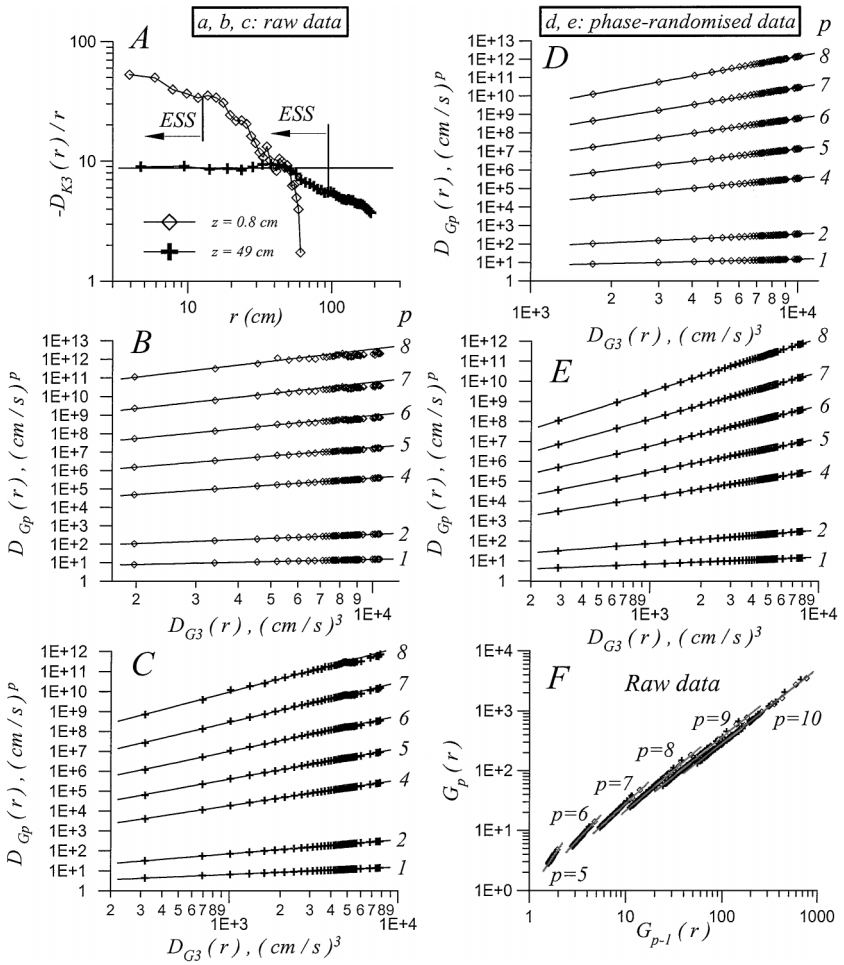

Figure 1. Structure functions of fluvial turbulence (Balmoral Irrigation Canal, New Zealand): A, normalized Kolmogorov's third-order structure functions measured at $z = 0.8$ cm and $z = 49$ cm; B and C, ESS plots for measurements at $z = 0.8$ cm and $z = 49$ cm, respectively; D and E, ESS plots for the same data as in B and C but after phase randomization; and F, G-ESS plots for both $z = 0.8$ cm and $z = 49$ cm.

different for different types of flows. However, for a particular flow class (e.g., the class of open channel flows) the function $f_1(r/L)$ is, probably, universal.

Figure 1F shows the same measurements using the G-ESS coordinates, G_p and G_q with $q = p - 1$, relationship (7). It is remarkable that all data, for both the high-shear near-bed region and the low-shear region, tightly collapse around

the same lines (in contrast to the ordinary ESS, Figs. 1B and 1C). The slopes of these lines, defined by least-square fitting (LSF), appear to be very close to exponents $\rho(p, p-1) = [\xi(p) - \xi(3)p/3]/[\xi(p-1) - \xi(3)(p-1)/3]$ with $\xi(p)$ from She and Leveque's (1994) model. Remarkably, the differences between these exponents and the LSF exponents decrease appreciably with increase in p, from 2.5% for $p = 5$ to 0.5% for $p = 10$. No systematic deviation of experimental points from the scaling lines was found, even at $r \gg L$, i.e., the G-ESS covers both the inertial subrange and large-scale velocity fluctuations equally well (compare with ESS in Figs. 1B and 1C, where points deviate from scaling lines at very large r). Note that such G-ESS behavior is consistent with (11).

SAND WAVES IN UNIDIRECTIONAL FLOWS

In this section we use results described in detail in Nikora and Goring (2000b).

Although sand waves are common features of river beds, sea floors, and terrestrial deserts, their scaling properties have been studied far less than those of turbulence. Probably the most substantial result was the discovery of the scaling law for the longitudinal wave number spectrum (Hino, 1968):

$$S(k) = \alpha(\phi)k^{-3} \quad \text{for } k_o \ll k \ll d^{-1} \tag{12}$$

where $k_o \propto H^{-1}$ is the low-bound wave number, H is the flow depth, d is the sand particle diameter, $\alpha(\phi)$ is a function of the angle of repose of sand particles, ϕ [$\alpha(\phi)$ was treated by Hino (1968) as a constant]. In contrast to turbulence scaling, no satisfactory explanation has been provided to justify $S(k) = \alpha(\phi)k^{-3}$, except simple dimensional arguments. The frequency spectra follows from (12) as

$$S(f) = \alpha(\phi)C^2 f^{-3} \tag{13}$$

where C is the analogue of phase velocity for sand waves, and f is frequency. Although relationship (12) has been confirmed in many laboratory and field studies, relationship (13) has been studied with much less details. In a recent study, Nikora, Sukhodolov, and Rowinski (1997) found that for wave lengths less than 0.15–0.25 of the flow depth, the sand wave propagation velocity C is inversely proportional to the wave length $l \sim k^{-1}$. When the wave lengths of spectral components are as large as 3–4 times the flow depth, no dispersion occurs, i.e., C does not depend on wave length. Nikora, Sukhodolov, and Rowinski (1997) suggested that these two ranges of scales (range 1 with $C \propto l^{-1} \propto k$ and range 2 with $C \propto l^o \propto k^o$) are due to the mechanism of sand wave movement. The small sand waves move due to the motion of individual sand particles (range 1) while larger sand waves (range 2)

propagate as a result of the motion of smaller waves on their upstream slopes. Just as the sand particles in the first type, these smaller waves redistribute sand from upstream slopes to downstream ones. Both types result in sand wave movement downstream but with different propagation velocity. Consequently, relationship (13) gives $S(f) \propto f^{-2}$ for range 1 and $S(f) \propto f^{-3}$ for range 2.

Using the above background we propose the following phenomenological model (Nikora and Goring, 2000b) that leads to Hino's "−3" law for the wavenumber spectrum and to "−2" and "−3" laws for the frequency spectrum. Moreover, this model allows multiscaling considerations similar to those for turbulence. We use the relationship for the wave energy dissipation rate ε as the basic relationship in the model, i.e.,

$$\varepsilon \propto g\frac{h_l}{T_l} = g\frac{h_l}{l}C(l) \tag{14}$$

where g is the gravity acceleration, h_l is the height of a sand wave with length-scale l, T_l is the "turnover time" associated with the scale l, and $C(l) = l/T_l$ is the wave propagation velocity. From (14) it immediately follows that

$$S(k) = \left\{\frac{\varepsilon}{gC(k)}\right\}^2 k^{-3} \tag{15}$$

and

$$S(f) = \left\{\frac{\varepsilon}{g}\right\}^2 f^{-3} = \left\{\frac{\varepsilon}{gC(k)}\right\}^2 C^2(k) f^{-3} \tag{16}$$

where we use $h_l \propto [S(k)k]^{0.5}$, ε may depend, in general, on $k \sim l^{-1}$, and $C \propto k \propto f^{0.5}$ is for range 1 and $C = \text{const}$ is for range 2. In the case of sand-wave self-similarity, $(h_l/l) = \text{const}$, which we assume for both range 1 and range 2, it follows that $(\varepsilon/gC) = \text{const}$ and thus "−2" and "−3" laws are recovered in (15) and (16), although with prefactors different from those in (12) and (13). This phenomenology also provides the relationships for the spatial $\langle|\Delta z|^p\rangle_l$ and temporal $\langle|\Delta z|^p\rangle_\tau$ structure functions. These follow straightforwardly from (14):

$$\langle|\Delta z|^p\rangle_l = a_p \left\langle \left\{\frac{\varepsilon}{gC}\right\}_l^p \right\rangle l^p \tag{17}$$

and

$$\langle|\Delta z|^p\rangle_\tau = a_p \left\langle \left\{\frac{\varepsilon}{g}\right\}_l^p \right\rangle \tau^p = a_p \left\langle \left\{\frac{\varepsilon}{gC}\right\}_l^p \right\rangle (C\tau)^p \tag{18}$$

where $\Delta z_l = [z(x+l,t) - z(x,t)] \sim h_l$ is the bed elevation increment between two points separated by distance l at fixed time t, $\Delta z_\tau = [z(x,t+\tau) - z(x,t)]$ is the difference in bed elevation at the same point after time lag $\tau \sim T_l$, a_p are constants that do not depend on l and τ, and the quantity $\{\varepsilon/gC\}_l$ is defined for the scale l. Relationship (17) for the spatial structure function is valid for both ranges 1 and 2, in similar fashion to (15). Relationship (18) gives two different relationships for these ranges, depending on the relationship for C:

$$\langle|\Delta z|^p\rangle_\tau = a_p \gamma^p \left\langle \left\{ \frac{\varepsilon}{gC} \right\}^p \right\rangle \tau^{p/2}, \quad C = \beta k = (\beta f)^{0.5} = \gamma \tau^{-0.5} \quad \text{range 1} \quad (19)$$

$$\langle|\Delta z|^p\rangle_\tau = a_p \left\langle \left\{ \frac{\varepsilon}{gC} \right\}^p \right\rangle C^p \tau^p, \quad C = \text{const} \quad \text{range 2} \quad (20)$$

where β and γ are some functions of flow variables that do not depend on k, f, l, and τ (Nikora, Sukhodolov, and Rowinski, 1997). For the ordinary scaling we have $\langle\{\varepsilon/gC\}^p\rangle \propto \langle\{\varepsilon/gC\}\rangle^p$, which means that $\langle\{\varepsilon/gC\}^p\rangle$ does not depend on l and τ. This case is analogous to nonintermittent turbulence, i.e., to K41. However, if the quantity $\{\varepsilon/gC\}$ is intermittent, similar to "intermittent" turbulence, we should expect $\langle\{\varepsilon/gC\}^p\rangle \propto \langle\{\varepsilon/gC\}\rangle^p l^{\chi_p}$, which gives, from (17), (19), and (20),

$$\langle|\Delta z|^p\rangle_l \propto l^{\xi_p = p + \chi_p} \quad \text{both ranges} \quad (21)$$

$$\langle|\Delta z|^p\rangle_\tau \propto \tau^{(\xi_p/2) = (p+\chi_p)/2} \quad \text{range 1} \quad (22)$$

$$\langle|\Delta z|^p\rangle_\tau \propto \tau^{\xi_p = p + \chi_p} \quad \text{range 2} \quad (23)$$

Thus, the model presented above may lead to either simple scaling with $\xi_p = p$ or to multiscaling with $\xi_p = p + \chi_p$. The type of scaling that occurs in nature should be defined from measurements.

For our ESS analysis of sand waves we have selected measurements of bed elevations with the highest sampling frequency available. They were made in the Buzau River (Romania), simultaneously at six points, with sampling interval 4 sec and sampling duration 17.5 hr. The details of these measurements may be found in Nikora, Sukhodolov, and Rowinski (1997). Figure 2A shows generalized structure functions of bed elevation with a well-defined scaling region at small τ, in agreement with (22). The same data presented in ESS coordinates, using the second order structure function as an argument, reveal two scaling regions, I and II, with slightly different slopes (Fig. 2B). The first region corresponds to the scaling region I in Figure 2A, while the second region covers the "nonscaling" points in Figure 2A, region II. Phase randomization of the raw data eliminate this difference (Fig. 2C). The origin of region II in Fig. 2B is not clear and is worth studying. The G-ESS plots (Fig. 2D) show nearly perfect scaling without crossover, as for

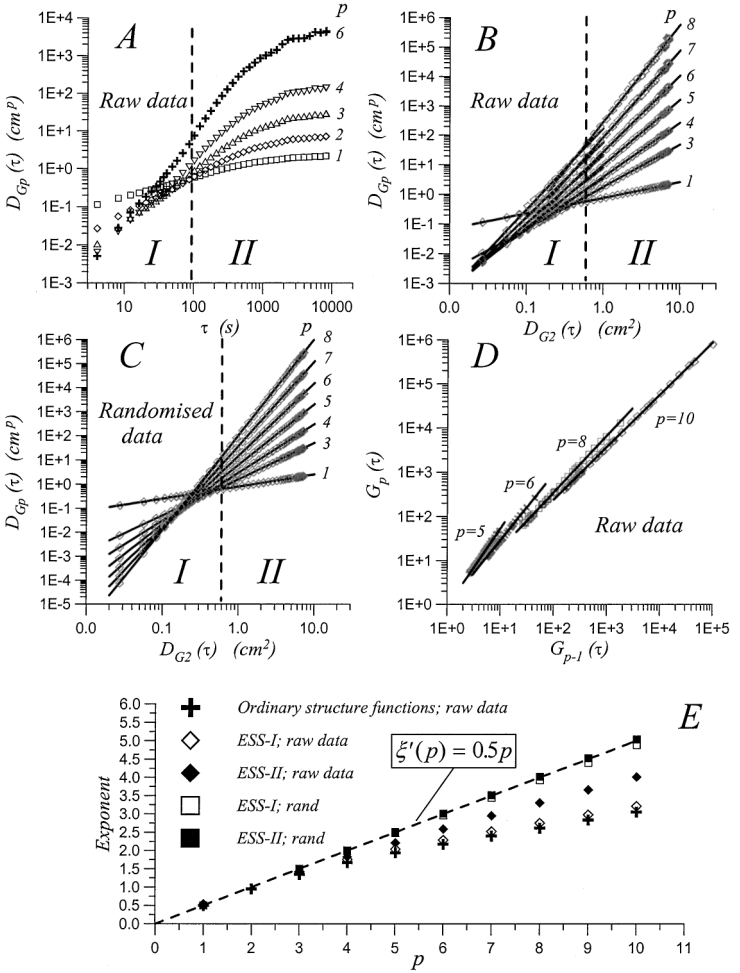

Figure 2. Structure functions of sand waves in unidirectional flow: A, generalised time structure functions of bed elevations; B and C, ESS plots for the raw and phase-randomized data, respectively; D, G-ESS plots for the raw data [note that we used $n = 2$ in relationship (8) when calculating G_p]; and E, the ordinary and ESS exponents vs order p.

turbulence data (Fig. 1F). The deviation of the exponents for the ordinary structure functions (Fig. 2A) and the ESS exponents for region I in Figure 2B from the nonintermittent exponents (Fig. 2E) is highly significant ($p_o \ll 0.01$). This result strongly supports the multiscaling nature of sand wave dynamics, i.e., relationships (21)–(23). The ESS exponents for the raw data in region II (Figs. 2B and E) also

deviate from nonintermittent behavior, though not so strongly as those for region I. The crossover in Figure 2B (i.e., the existence of two scaling regions, I and II) is unexpected and may reflect some interesting dynamics.

OTHER EXAMPLES

The following subsections present pilot ESS examples rather than comprehensive scaling analyses based on developed phenomenology. Therefore, we restrict our considerations to the ESS existence and intermittency identification only.

Martian Surface

In 1998 the Mars Global Surveyor entered stable orbit around mars. During a hiatus in aerobraking the Mars Orbiter Laser Altimeter was turned on and 34 topography tracks were recorded. We explore here track no. 24, which passed from south to north over the northwestern flank of Olympus Mons, the highest mountain in the solar system. The fractured lava, which is a feature of the flanks of Olympus Mons, was captured in fine detail at intervals of 0.0076 degrees of latitude (0.45 km), over length of 540 km. The data used in this study were pre-processed by fitting a quardic to remove the large-scale features. Figure 3 summarizes the ESS analysis for this profile. The raw ESS exponents deviate from those for the phase-randomized data only slightly, although the difference between them is statistically significant ($p_o < 0.01$). This agrees well with nearly linear dependence ξ_p on p for generalized structure functions, which may be approximated as $\xi(p) = 0.86p$ (Fig. 3E). The G-ESS plots show excellent scaling within the whole range of scales investigated (Fig. 3D).

River Morphometry

It is well known that river depth and width fluctuate downstream due to intrachannel and floodplain morphological forms. These fluctuations have been well studied in fluvial geomorphology, although they still await a comprehensive quantitative analysis. Here we apply the ESS concept to analyze the downstream fluctuations of the maximum flow depth (i.e., the thalweg depth). We use data for the Prut River (Moldova), collected from small-scale hydrographic (bathymetric) maps at a sampling interval of 50 m, which is less than the river width. The reach length was 327.55 km. Figure 4 summarizes the ESS analysis for these data and clearly demonstrates properties similar to those revealed for sand waves (Fig. 2), including strong intermittency and the existence of two scaling regions in the ESS plots.

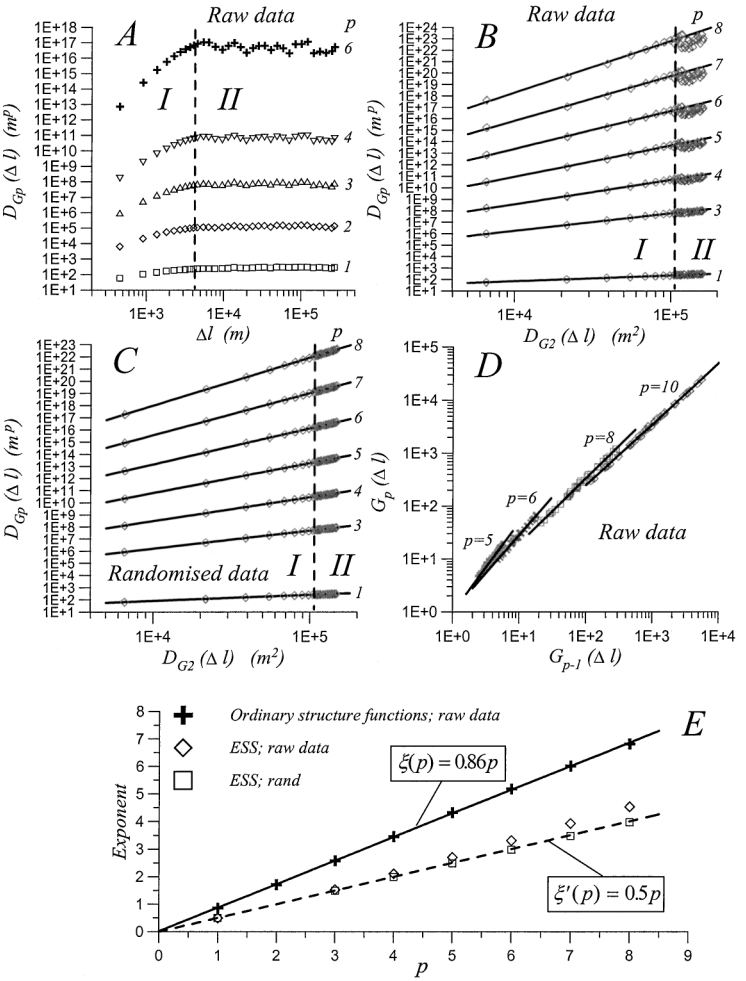

Figure 3. Structure functions of Martian topography (the flanks of Olympus Mons): A, generalised spatial structure functions of surface elevations; B and C, ESS plots for the raw and phase-randomized data, respectively; D, G-ESS plots for the raw data [note that we used $n = 2$ in relationship (8) when calculating G_p]; and E, the ordinary and ESS exponents vs order p.

Gravel-Bed Mobility

In this example we use data from underwater video records in the Balmoral Irrigation Canal, which were made to support our turbulence measurements. The

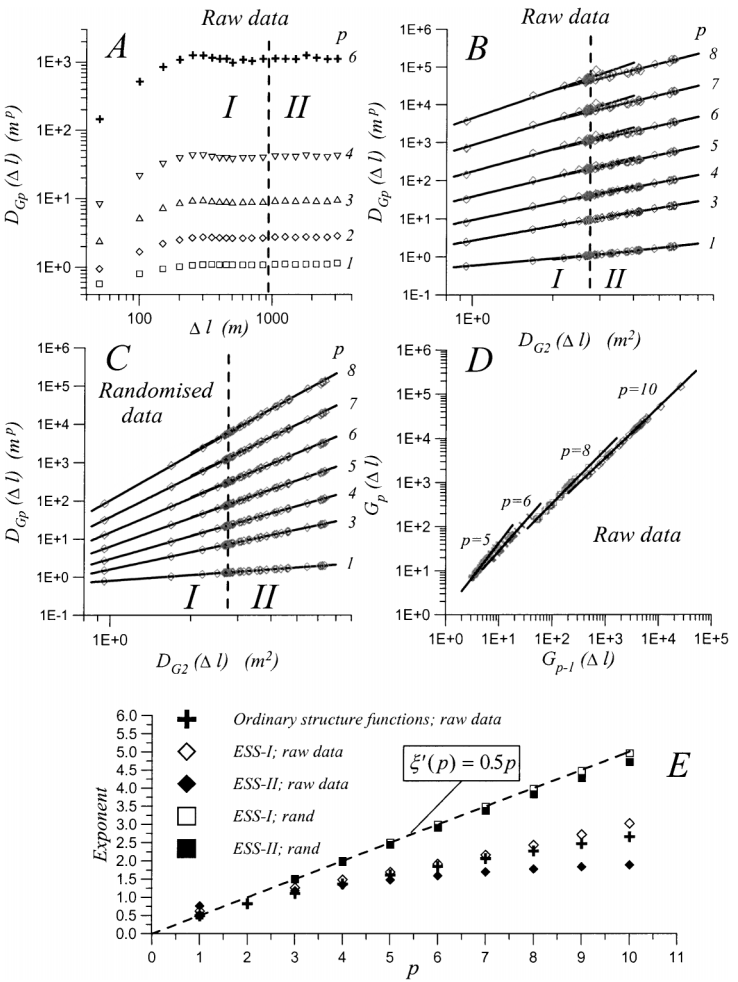

Figure 4. Structure functions of the flow depth (Prut River, Moldova): A, generalized spatial structure functions of depths along the river; B and C, ESS plots for the raw and phase-randomized data, respectively; D, G-ESS plots for the raw data [note that we used $n = 2$ in relationship (8) when calculating G_p]; and E, the ordinary and ESS exponents vs order p.

details of these measurements may be found in Nikora and Goring (2000c). The quantity that we analyze here is the number of mobile bed particles within a selected bed area, sampled with the interval 0.16 sec. The duration of the time record used was 27 min. The ESS summary of these data is presented in Figure 5,

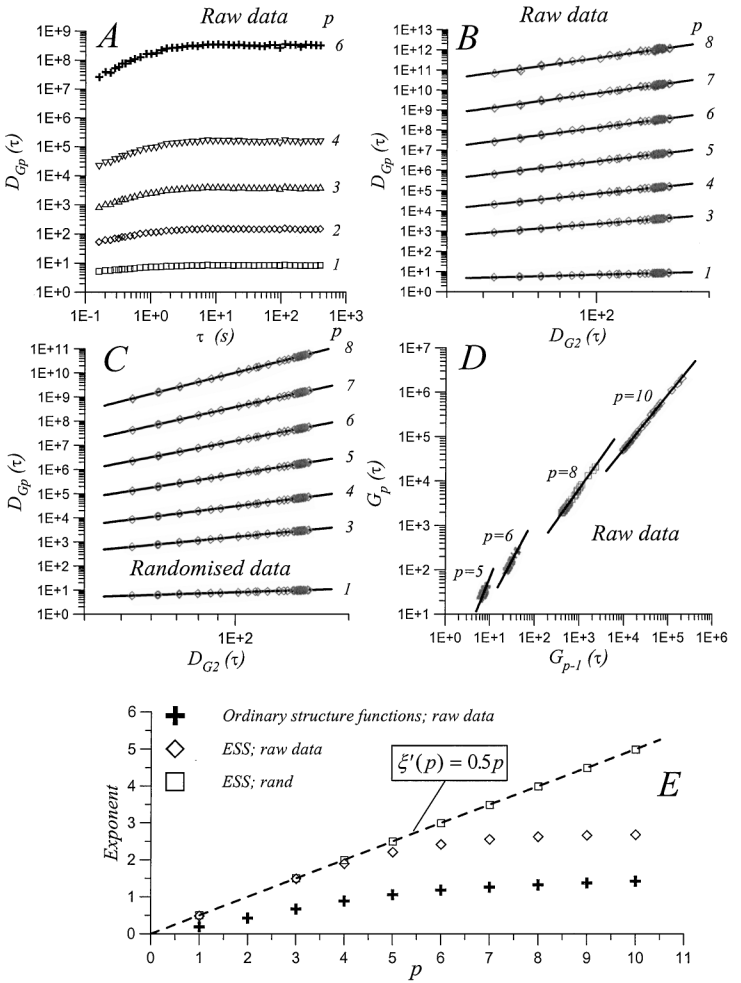

Figure 5. Structure functions of bed mobility (Balmoral Irrigation Canal, New Zealand): A, generalized time structure functions of relative number of mobile bed particles; B and C, ESS plots for the raw and phase-randomized data, respectively; D, G-ESS plots for the raw data [note that we used $n = 2$ in relationship (8) when calculating G_p]; and E, the ordinary and ESS exponents vs order p.

which clearly shows the applicability of the ESS concept and strongly suggests a multiscaling nature of the observed intermittent bed load ($p_o \ll 0.01$). This intermittency is driven, most probably, by intermittent turbulent events in the near-bed region.

Barometric Pressure

Our last example relates to atmospheric pressure fluctuations measured in Christchurch (New Zealand) from 1996 to 1999, with a sampling interval of 5 min. The measured fluctuations are probably due to gravitational waves and synoptic variability since turbulence related fluctuations usually occur with periods smaller than 5 min (Monin and Yaglom, 1975). The generalized structure functions in Figure 6A do not reveal a clear scaling region, in contrast to the previous examples. Therefore, the scaling exponents for the generalised structure functions were estimated for a selected region (dashed area in Fig. 6A) where the local slope $d \ln D_{Gp}/d \ln \tau$ was nearly constant for p from 1 to 10. The ESS plots for the raw data also show some deviations from straight lines, especially for large p (Fig. 6B). These deviations may be an effect of superposition of fluctuations generated by different mechanisms. However, in spite of these deviations in the ESS plots, the G-ESS plots (Fig. 6D) appeared to be as good as in the previous examples. Also, Figure 6E shows that pressure fluctuations may be considered as nearly nonintermittent, as $\xi(p)$ may be fairly well approximated as a linear function $\xi(p) = 0.867p$.

DISCUSSION AND CONCLUSIONS

For all of the examples of geological and geophysical phenomena that we considered, we found that data presentation in ESS coordinates reveals scaling behavior over a much wider range of scales than observed in conventional coordinates. This helped to identify strong intermittent behavior in fluvial turbulence, sand wave dynamics, river morphometry, and gravel-bed mobility, which is expressed by nonlinearity in the function $\xi'(p)$. However, two examples, Martian topography and atmospheric pressure, showed "nearly nonintermittent" scaling. Such a test for intermittency is important when one is interested in understanding underlying mechanisms. For example, we showed for the case of sand waves that a simple phenomenological model may lead to either ordinary scaling or multiscaling. The ESS analysis strongly supports the latter, suggesting complex dynamics that possibly involve intermittency in the wave energy dissipation.

However, the most striking result of our analysis is that the G-ESS plots for all examples appear to be very similar and reveal global scaling behavior, i.e., within the whole range of scales investigated. Moreover, all data collapse on the same lines when plotted together (Fig. 7). This was unexpected as the G-ESS concept has been originally justified for turbulence, i.e., involving turbulence phenomenology (Benzi and others, 1996). This phenomenology is quite specific and is unlikely to be universally applicable. An explanation for the unexpected behavior of the G-ESS plots in our study is that the probability distributions of the signal

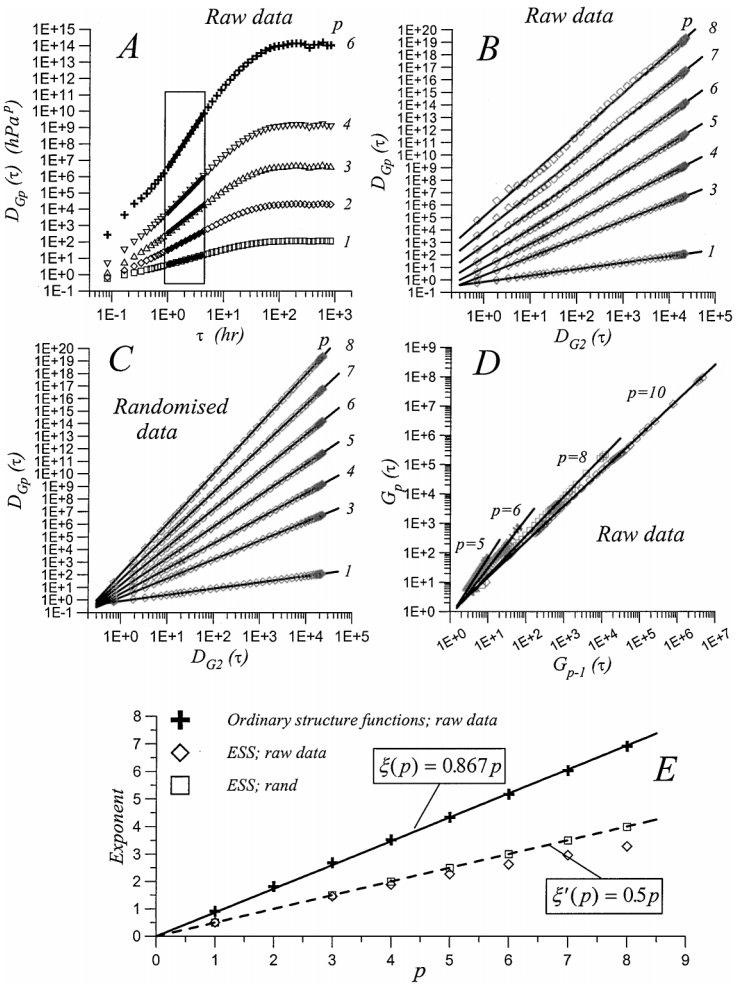

Figure 6. Structure functions of atmospheric barometric pressure (Christchurch, New Zealand): A, generalized time structure functions of barometric pressure; B and C, ESS plots for the raw and phase-randomized data, respectively; D, G-ESS plots for the raw data [note that we used $n = 2$ in relationship (8) when calculating G_p]; and E, the ordinary and ESS exponents vs order p.

increments for the phenomena we studied may be similar, and this similarity resulted in the universality of the G-ESS plots. This explanation can find support in Bershadskii (1996), who suggested a concept for turbulence G-ESS using the probability distributions for velocity increments rather than involving turbulence phenomenology.

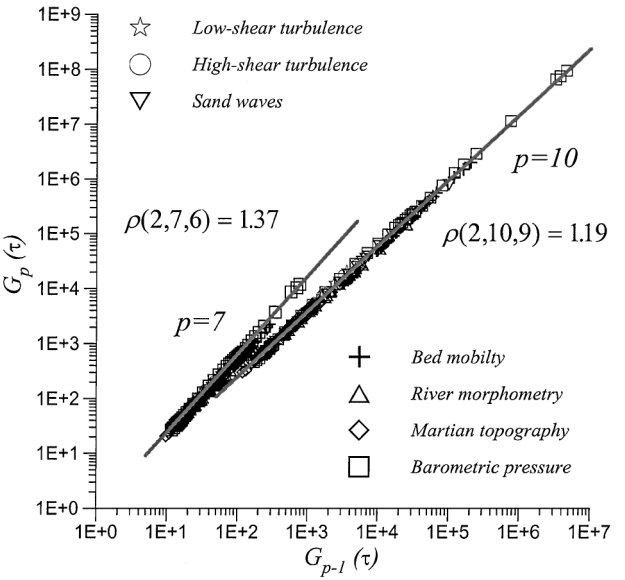

Figure 7. Summary G-ESS plots showing that all data considered collapse on the same lines. Only points for $p = 7$ and $p = 10$ are shown for clarity.

Finally, our considerations suggest that, indeed, ESS and G-ESS may be an inherent property of many natural phenomena rather than a property exclusively of turbulence.

ACKNOWLEDGMENTS

The study was conducted under Contract NIW701 from the Marsden Fund, administered by the Royal Society of New Zealand. We are grateful to B. S. Daya Sagar for the invitation to submit a paper to this issue. C. P. Pearson, and D. M. Hicks provided helpful comments, which we gratefully incorporated into the final article. Many colleagues at NIWA, USGS, Institute of Geophysics and Geology of Academy of Science of Moldova, and Research Station Stejarul (Piatra Neamt, Romania) helped with data collection and preliminary data analyses.

REFERENCES

Avnir, D., Biham, O., Lidar, D., and Malcai, O., 1998, Is the geometry of nature fractal?: Science, v. 279, p. 39–40.

Barenblatt, G. I., 1979, Similarity, self-similarity, and intermediate asymptotics: Plenum Press, New York, 218 p.

Biferale, L., Benzi, R., and Pasqui, M., 1997, Generalised scaling in turbulent flows, *in* Boratav, O., Eden, A., and Erzan, A., eds., Turbulence modeling and vortex dynamics: Springer-Verlag, Berlin, p. 74–91.

Bendat, J. S., and Piersol, A. G., 1986, Random data: Analysis and measurement procedures: John Wiley & Sons, New York, 566 p.

Benzi, R., Biferale, L., Ciliberto, S., Struglia, M. V., and Tripiccione, R., 1996, Generalised scaling in fully developed turbulence: Phys D, v. 96, p. 162–181.

Benzi, R., Ciliberto, S., Baudet, C., Chavarria, G. R., and Tripiccione, R., 1993a, Extended self-similarity in the dissipation range of fully developed turbulence: Europhys Lett, v. 24, no. 4, p. 275–279.

Benzi, R., Ciliberto, S., Tripiccione, R., Baudet, C., Massaioli, F., and Succi, S., 1993b, Extended self-similarity in turbulent flows: Phys Rev, v. E 48, p. R29–R32.

Bershadskii, A., 1996, Pseudo-scaling in laboratory and in numerical simulations of turbulence: Journal of Physics A: Mathematical and General, v. 29, p. L453–L458.

Davis, J. C., 1986, Statistics and data analysis in geology: John Wiley & Sons, New York, 646 p.

Frisch, U., 1995, Turbulence. The legacy of A. N. Kolmogorov: Cambridge University Press, Cambridge, 296 p.

Goring, D. G., and Nikora, V. I., 1999, Phase-randomisation and phase-synhronisation as turbulence analysis tools: Proc. of XXVII IAHR Congress (CD-ROM), Graz, Austria, Aug. 22–27, 1999; p. 237 in the Abstract Volume.

Hino, M., 1968, Equilibrium-range spectra of sand waves formed by flowing water: Journal of Fluid Mechanics, v. 34, p. 565–573.

Kundagrami, A., Dasgupta, C., Punyindu, P., and Das Sarma, S. 1998, Extended self-similarity in kinetic surface roughening: Phys Rev E, v. 57 no. 4, p. R3703–R3706.

Kraus, N. C., Lohrmann, A., and Cabrera, R., 1994, New acoustic meter for measuring 3D laboratory flows: Journal of Hydraulic Engineering, ASCE, v. 120, no. 3, p. 406–412.

Monin, A. S., and Yaglom, A. M., 1975, Statistical fluid mechanics: Mechanics of turbulence, v. 2: MIT Press, Boston, MA, 874 p.

Nikora, V. I., and Goring, D. G., 1998, ADV turbulence measurements: Can we improve their interpretation?: Journal of Hydraulic Engineering, ASCE, v. 124(6), p. 630–634.

Nikora, V., and Goring, D., 1999a, On the relationship between Kolmogorov's and generalised structure functions in the inertial subrange of developed turbulence: Journal of Physics A: Mathematical and General, v. 32, p. 4963–4969.

Nikora, V. I., and Goring, D. G., 1999b, Effects of bed mobility on turbulence structure: NIWA Internal Report No 48, Christchurch, 48 p.

Nikora, V. I., and Goring, D. G., 2000a, Eddy convection velocity and Taylor's hypothesis of 'frozen' turbulence in a rough-bed open-channel flow: J. HydroScience and Hydraulic Engineering, JSCE, v. 18(2), p. 75–91.

Nikora, V. I., and Goring, D. G., 2000b, Sand waves in unidirectional flows: Scaling and intermittency: Physics of Fluids, AIP, v. 12(3), p. 703–706.

Nikora, V. I., and Goring, D. G., 2000c, Flow turbulence over fixed and weakly mobile gravel beds: J. Hydraulic Engineering, ASCE, v. 126(9), p. 679–690.

Nikora, V. I., Sukhodolov, A. N., and Rowinski, P. M., 1997, Statistical sand wave dynamics in one-directional water flows: Journal of Fluid Mechanics, v. 351, p. 17–39.

Queiros-Conde, D., 1997, Geometrical extended self-similarity and intermittency in diffusion-limited aggregates: Physical Review Letters, v. 78(23), p. 4426–4429.

She, Z.-S., and Leveque, E., 1994, Universal scaling laws in fully developed turbulence: Physical Review Letters v. 72, p. 336–339.

Turcotte, D. L., 1997, Fractals and chaos in geology and geophysics: Cambridge University Press, Cambridge, 398 p.

Turiel, A., Mato, G., and Parga, N., 1998, Self-similarity properties of natural images resemble those of turbulent flows: Physical Review Letters, v. 80(5), p. 1098–1101.

Yamada, M., and Ohkitani, K., 1991, An identification of energy cascade in turbulence by orthonormal wavelet analysis: Progress of Theoretical Physics, v. 86, p. 799–815.